J. Water Environ. Nanotechnol., 6(4): 356-366 Autumn 2021

ORIGINAL RESEARCH PAPER

Laser Scribed Graphene from Oil Palm Lignin for Supercapacitor Applications

Narasimhaa Naidu Loganathan [1,2] *, Kabilashen Readdyi Munusamy [1,2], Veeradasan Perumal [1,2], Bothi Raja Pandian [3]

[1] entre of Innovative Nanostructure and Nanodevices (COINN), Universiti Teknologi PETRONAS (UTP), 32610 Seri Iskandar, Perak Darul Ridzuan, Malaysia.
[2] Department of Mechanical Engineering, Universiti Teknologi PETRONAS (UTP), 32610 Seri Iskandar, Perak Darul Ridzuan, Malaysia.
[3] School of Chemical Sciences, Universiti Sains Malaysia, Gelugor 11800, Pulau Pinang, Malaysia.

Received: 2021-05-17 Accepted: 2021-07-12 Published: 2021-08-01

ABSTRACT
This paper reports a facile carbonization method of a biopolymer to synthesize reduced graphene oxide with excellent electrochemical properties for use as a supercapacitor electrode. Oil palm lignin is used as the biopolymer-based graphene precursor, and a carbon dioxide laser is used to carbonize the material via lithography. Using Raman Spectroscopy, the characterization of the resultant graphene (OP-LSG) revealed D, G, and 2D peaks corresponding to multilayer graphene. Scanning Electron Microscopy of OP-LSG revealed three-dimensional particle-like fibrous and porous nanostructures with an enhanced surface area. In a three-electrode setup in ferrocyanide electrolyte, cyclic voltammetry showed the electrode coated with OP-LSG achieving a specific capacitance as high as 108.044 mF/cm^2 at a scan rate of 0.01 V/s. The galvanostatic charge-discharge of OP-LSG revealed energy and power density values of 15 µWh/cm^2 and 597 µW/cm^2 at a scan rate of 0.01 V/s. The OP-LSG electrode retained 97.5% of its initial capacitance after 1000 charge-discharge cycles.

Keywords: *Reduced graphene oxide, electric double layer capacitor, laser lithography, graphene electrode, biopolymer*

How to cite this article
Naidu Loganathan N., Readdyi Munusamy K., Perumal V., Raja Pandian B. Laser Scribed Graphene from Oil Palm Lignin for Supercapacitor Applications. J. Water Environ. Nanotechnol., 2021; 6(4): 356-366.
DOI: 10.22090/jwent.2021.04.006

INTRODUCTION

Supercapacitors, or ultracapacitors, are capacitors that can achieve high power outputs at lower operating voltages [1]. They are able to bridge the gap between rechargeable batteries and electrolytic capacitors by having a higher power input and output, as well as many more charge and discharge cycles than the former but a higher energy density than the latter [2]. Supercapacitors do not use the conventional solid dielectric, instead, they use either electrostatic double-layer capacitance or electrochemical pseudocapacitance, or both. There are three types of supercapacitors, Electric Double Layer Capacitors (EDLC), pseudocapacitors, and hybrid supercapacitors. Although all three types of supercapacitors are constructed of similar components, i.e., anode, cathode, separator, electrolyte, and current collectors, their energy storage mechanism differs based on the configuration of electrodes (i.e., anode, cathode) used. EDLC has electrodes that are made from carbon-based materials. True to its name, the energy storage mechanism in EDLC is via a Helmholtz double layer between the surface of the electrode and the electrolyte. In contrast,

* Corresponding Author Email: *narasimhaa_20001679@utp.edu.my*

pseudocapacitors store charges electrochemically by swapping out the carbon-based electrodes in EDLC to redox-active materials, to allow reduction and oxidation within the electrode, intercalation or electrosorption. Hybrid supercapacitors combine both EDLC and pseudocapacitors' characteristics, by using a combination of a redox-active electrode and a carbon-based electrode.

Electrodes play a significant role in determining the performance of the supercapacitor. EDLC possesses better power densities and capacitance due to the large surface area of the carbon-based electrodes [1]. Capacitance can be further increased by swapping the conventional carbon electrodes to materials with better physical properties, i.e., enhanced porosity and larger surface area such as graphene, due to its excellent properties such as high electron mobility and excellent electrical conductivity, owing to its honeycomb arrangement in a monolayer thickness atom [3,4]. These properties, combined with the large specific surface area, make graphene a better material for the fabrication of supercapacitor electrodes than traditional carbon-based materials [5].

However, the synthesis of pristine graphene via traditional methods, i.e., mechanical exfoliation, chemical exfoliation, chemical vapor deposition (CVD), is not viable due to multiple factors. Mechanical exfoliation is not scalable for mass-production as it requires layer-by-layer exfoliation of graphite using an adhesive [5,6] with process optimization limited to force control of the exfoliation [5,7]. Chemical exfoliation requires graphite to be submerged in an alkaline solution to chemically induce separation between the graphene layers. This method produces graphene which is not uniform, affecting the electron mobility of the material [5]. In CVD, graphite is heated to ultra-high temperatures, effectively transforming it into a gaseous state. The gas is then used to grow a thin film of graphene on a substrate [5,8]. Although CVD is deemed the most feasible method for mass production, it requires high initial investments and running costs.

Hence, studies have been done on reduced Graphene Oxide (rGO) synthesized by reduction of a carbon precursor. Previously, researchers have utilized both chemical and electrochemical reduction routes to synthesize multilayer graphene [9]. Although the electrochemical route resulted in good graphene yield, the process still requires an exfoliation step and reducing agents to synthesize graphene. Recently, laser lithography has been used to scribe and reduce graphene oxide to rGO using a carbon dioxide laser [10]. The high-heat laser pulse uses a photo-thermal effect to excite the oxide bond of graphene oxide [11,12], effectively converting the sp^3 carbon atoms to sp^2 carbon atoms. A critical fluence rate is required to start the carburization process to burn the oxygen-containing functional group from the graphene oxide layer, leaving behind the rGO with a three-dimensional structure [10,13,14]. This process comprises both reduction and exfoliation of the graphene oxide into a single step, without the need for any additional reducing agents. This method is economical as it does not require binders, post-treatment, or chemical processing.

The three-dimensional structure of the rGO results in a higher specific surface area and porosity than conventionally synthesized graphene e.g., CVD, mechanical exfoliation. Polymers have been widely used in the development of supercapacitor components due to their excellent characteristics [15–18]. Most studies have used synthetic polymers such as polyimide as a precursor for graphene synthesis via laser lithography [14,19–21]. However, in recent years, development has been focused on using biopolymers such as cellulose and alginate as precursors in rGO synthesis, due to their low cost and sustainability. Lignin, which comprises the lignocellulosic biopolymer that provides strength to the cell wall of plants along with cellulose and hemicellulose, is a promising biopolymer [22]. Multiple types of lignin e.g.., pulpwood lignin, Kraft lignin, lignosulfonate, [23–26] have previously been used in the development of supercapacitor components. In this paper, we report the synthesis of rGO from an oil palm lignin precursor via laser lithography, and its subsequent application as a viable supercapacitor electrode material due to its unique three-dimensional structure with higher specific surface area and porosity as compared to previously researched forms of lignin. The use of oil palm lignin as a precursor for synthesizing graphene has not been reported previously in any studies.

MATERIALS AND METHODS

Lignin powder is extracted from oil palm fronds using a rotary digester machine based on a soda pulping process [27]. 500 g of biomass is added to the digester, followed by 30% (w/v) aqueous sodium hydroxide and water. The ratio of biomass

to water to aqueous sodium hydroxide is 1:6:2. The digester is set at 170°C, and the mixture is cooked for 3 hours at 10 to 11 bars. Upon completion of the pulping process, the pulp is left to cool overnight. The pulp is then filtered with a metal sieve, followed by vacuum-assisted filtration via a Buchner funnel, to remove residues. The resultant material, black liquor, is highly alkaline, with a pH value between 13 to 14. The lignin is precipitated from the alkaline black liquor by acidification using 20% (v/v) sulfuric acid. Once the solution's pH level has been reduced to 2, it is stored overnight in a refrigerator for layer separation.

The precipitated lignin is centrifuged at 3500 rpm for 10 minutes to eliminate excess water and dried inside an oven at 50°C for five days to remove residual moisture. The material is then ground to form lignin powder and refluxed with n-pentane via Soxhlet apparatus for 6 hours at 40°C. This step is required to remove lipophilic non-lignin materials such as wax and lipids from the powder. The lignin is filtered and washed with distilled water acidified using sulfuric acid until the solution reaches a pH level of 2 to remove n-pentane and non-lignin phenolic compounds from the pulping and purification process. The thoroughly purified lignin is dried inside an oven for 24 hours to produce ready-to-use lignin powder.

The **lignin solution** for laser lithography is prepared by diluting 10 grams of the lignin powder in 100 milliliters of distilled water. The solution is then stirred magnetically on a hot plate for 30 minutes to ensure uniform and homogenous lignin dispersion. The resulting lignin solution has a 10 percent concentration of lignin.

The lignin solution is subsequently dropped cast on the substrate. 20mm by 20mm glass substrates are decontaminated using ethanol solution, and the electrical conductivity of the substrate is measured using a multi-meter to ensure the surface of the substrate is non-conductive. The lignin solution is then dropped cast to cover the entire surface of the substrate. To ensure a uniform layer of solution on the substrate and to remove excess solution, the Doctor Blade technique is performed by placing a sharp blade at a fixed distance from the surface of the substrate to ensure a coating with even thickness. The coated substrate is then dried at 50°C for 20 minutes to prepare the surface for subsequent coating layers. Once the drying is completed, the substrate is cooled down to room temperature before subsequent applications of lignin coatings are performed using the same method described above. The process is repeated until ten layers of lignin films are deposited on the glass substrate.

Next, **laser lithography** is performed on the coated substrate using a CO_2 laser under ambient conditions [14]. A V460 Universal Laser Engraver machine is used for the laser lithography process. The scribing is done using a raster scan method with the laser configuration set at 18 W power, 50% speed, and 500 pulses per inch (PPI) resolution. The coated substrate darkens upon laser scribing, an indication that graphene has formed through the carburization process.

Material characterization of the resulting OP-LSG via Raman spectroscopy was done using a Horiba Jobin Yvon HR800 Raman Spectrometer, to determine the chemical structure, phase, polymorphy, crystallinity, and molecular interactions of the OP-LSG. The sample was scraped from the glass substrate and analyzed using the Raman spectroscope. The laser wavelength for the spectroscope was set at 532nm [10,28], and the achromatic lens was focused on the OP-LSG. The surface morphology of the sample was obtained using a Zeiss Supra 55 VP Field-Emission Scanning Electron Microscope. The Scanning Electron Microscopy (SEM) was performed on both the lignin-coated glass substrate and the OP-LSG, to compare the different surface morphologies pre- and post-laser lithography.

For the **electrochemical performance analysis** of the OP-LSG, a Metrohm DropSens C110 screen-printed electrode (SPE) setup was used [29,30] to analyze OP-LSG's viability as a supercapacitor electrode. The SPE setup is made up of three electrodes, a working electrode (WE) made of carbon with a diameter of 4 mm, a reference electrode (RE) made of silver, and an auxiliary/counter electrode (CE) made of carbon. The working electrode's surface is modified with 10 µL of OP-LSG mixed with a complex solution, as shown in Fig. 1(a) below. The complex solution is made by diluting 2% (3-Aminopropyl) triethoxysilane, APTES, in pure Ethanol. 5mM of 16-Mercaptohexadecanoic acid and 50mM N-Hydroxysuccinimide were subsequently added, and the solution was stirred at room temperature with 200mM 1-Ethyl-3-(3-dimethylaminopropyl) carbodiimide added to the solution. This complex solution allows the dispersion of the OP-LSG for it to be coated on the surface of the WE in the SPE.

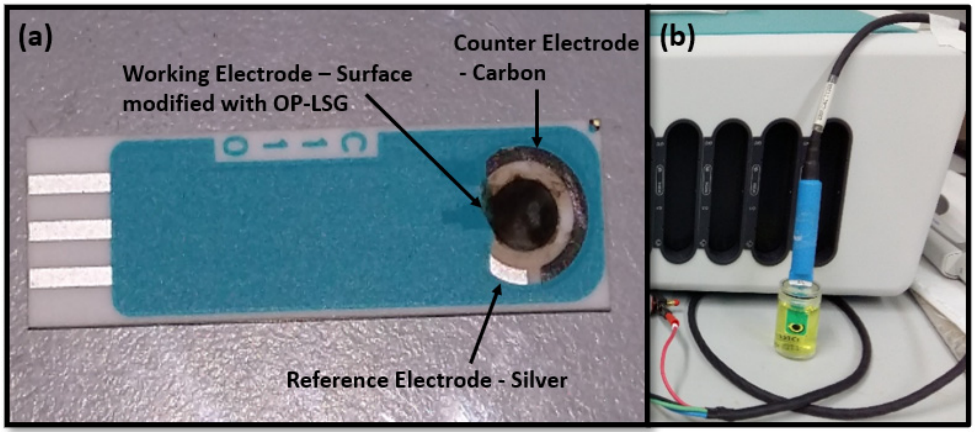

Fig. 1. (a), The SPE chip with surface modified OP-LSG working electrode, carbon counter electrode, and silver reference electrode. (b), The modified SPE chip in a ferrocyanide electrolyte solution for electrochemical performance testing of the OP-LSG electrode.

The surface modification is performed in a fume hood, to prevent impurities in the electrode surface. The diameter of the modified working electrode is 4mm, with a working electrode active surface area of 0.1257cm^2 for interaction with the electrolyte.

The electrochemical analysis is performed using a three-electrode configuration to measure the potential of the working electrode versus the reference electrode [31,32], as the two-electrode setup only allows the measurement of the potential difference between the anode and cathode. A 5nM ferrocyanide electrolyte is used, as shown in Fig. 1(b) below [24,33] to ensure no unwanted reaction between the electrode and electrolyte.

Electrochemical Impedance Spectroscopy (EIS) was then performed on this setup using a Metrohm Autolab PGSTAT302N potentiostat/galvanostat, to determine the conductivity and the impedance of the OP-LSG electrode based on a phase angle plot and Nyquist Impedance plot of 1 MHz to 50 Hz with 10 frequencies per decade, and a 0.1 V_{RMS}. A potentiostat Cyclic Voltammetry (CV) scan from 0mV to 5mV was performed on the three-electrode setup using the same instrument to determine the capacitance of the electrode. The voltage window, which is the difference between the upper and lower vertex, was kept at 1 V. A Galvanostatic Charge-Discharge (GCD) test to determine the charge-discharge and cycling stability of the OP-LSG electrode was performed on the three-electrode setup using the same instrument, at 0A, with an upper vertex of 1mA and a lower vertex of -1mA and a scan rate of 1 to 50mA per cm^2.

The areal specific capacitance of the OP-LSG electrode is calculated from the CV curves based on Equation S1 below:

$$Specific\ Capacitance, C_S = \frac{\int_{V_i}^{V_f} I\ dV}{2 \times S \times k \times \Delta V} \quad \text{Eq. S1 [34]}$$

Where,

$\int_{V_i}^{V_f} I\,dV$ = Integrated area of the CV curve (in AV)
S = Surface area of the electrode (in cm^2)
k = Scan rate (in V/s)
ΔV = Potential Window ($V_f - V_i$) (in V)

The energy and power densities are calculated from the GCD curves based on Equations S2 – S3 below. Further, the specific capacitance is also computed based on Equation S4 using the GCD curves to determine the capacitance retention rate of the electrode after 1000 charge-discharge cycles.

$$Specific\ Energy\ Density, E_S = \frac{1}{2} \times C_A \times \frac{(\Delta V)^2}{3600} \quad \text{Eq. S2 [34]}$$

Where,
C_A = Specific Capacitance from GCD
ΔV = Discharge Potential from GCD

$$Specific\ Power\ Density, P_S = \frac{E_S}{\Delta t} \times 3600 \quad \text{Eq. S3 [34]}$$

Where,
E_S = Specific Energy Density
Δt = Discharge time (in seconds)

$$Areal\ Specific\ Capacitance, C_A = \frac{1}{S \times \frac{dV}{dt}} \quad \text{Eq. S4}$$

Where,

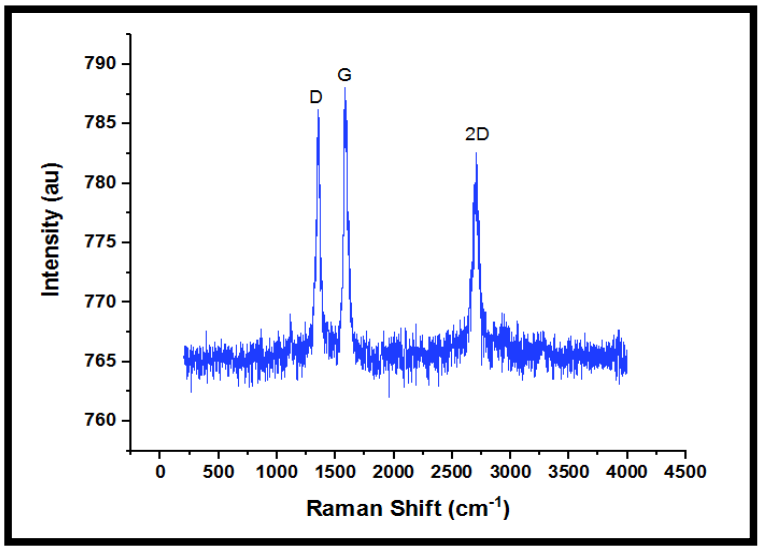

Fig. 2. Raman spectrum plot of OP-LSG.

S = Surface area of the electrode (in cm^2)
$\frac{dV}{dt}$ = Slope of the GCD Curve

RESULTS AND DISCUSSION

Fig. 2 shows the Raman spectrum of the OP-LSG where three significant peaks were observed. The first peak in the Raman shift is known as the D-band, which occurs at 1450 cm^{-1}. The second peak is the G-band, which occurs at 1600 cm^{-1}, and the third peak, known as the 2D band, occurs at 2700 cm^{-1}. All three peaks occur within the range associated with graphene [28], thereby confirming the presence of graphene from the laser lithography of oil palm lignin.

The formation of the D band peak between 1400 to 1570 cm^{-1} suggests the presence of defected graphite with distorted surface morphology in sp^2 hybridized carbon atoms since the D-band originates from the hybridized vibrational mode of the graphene edges and dis-ordered structures [35–37]. The use of laser would result in structural edge defects and a corresponding D-band peak [33,38]. Hence, the D-peak observed here is most likely from the over-carburization of the lignin at the edge of the glass substrate, since the coating would be thinner there. Due to the thinner lignin, the edge of the substrate would undergo a higher degree of graphitization, leading to the defective structure indicated in the OP-LSG Raman plot.

On the other hand, the intensity of the 2D peak and the G peak in the Raman plot indicates the successful conversion of lignin into multilayer graphene [39]. The D band to G band ratio has previously been used to identify the degree of crystallization and the defect density of carbon materials [40]. For OP-LSG, the ratio of I_D/I_G is 0.81. This indicates the presence of defects in the three-dimensional structure of the OP-LSG. A potential source of defect present in the OP-LSG, other than the substrate edge defect, could be the under-graphitization of the lignin coating in the glass substrate. The lower layers of the lignin coating could experience a lower degree of graphitization during the laser lithography process, hence the presence of under-graphitized lignin in OP-LSG. With the Raman plot indicative of the formation of three-dimensional graphene in the OP-LSG, it is important to view the corresponding surface topology and the material's morphology.

As can be seen from Fig. 3 (a), (b), (c), the FESEM images of the lignin coating pre-laser lithography indicate a tightly packed structure with irregularities. These irregularities could be attributed to lignin molecules that were not fully dispersed in the solution. There are also voids indicated in the structure of the lignin, possibly due to the evaporation of water in the lignin coating layers before the laser lithography process [41,42]. Figs. 3 (d), (e), (f) show the presence of a fibrous structure on the surface of the OP-LSG, at different resolutions.

The three-dimensional OP-LSG has a high degree of porosity due to the carburization of the lignin when the carbon dioxide laser beam strikes

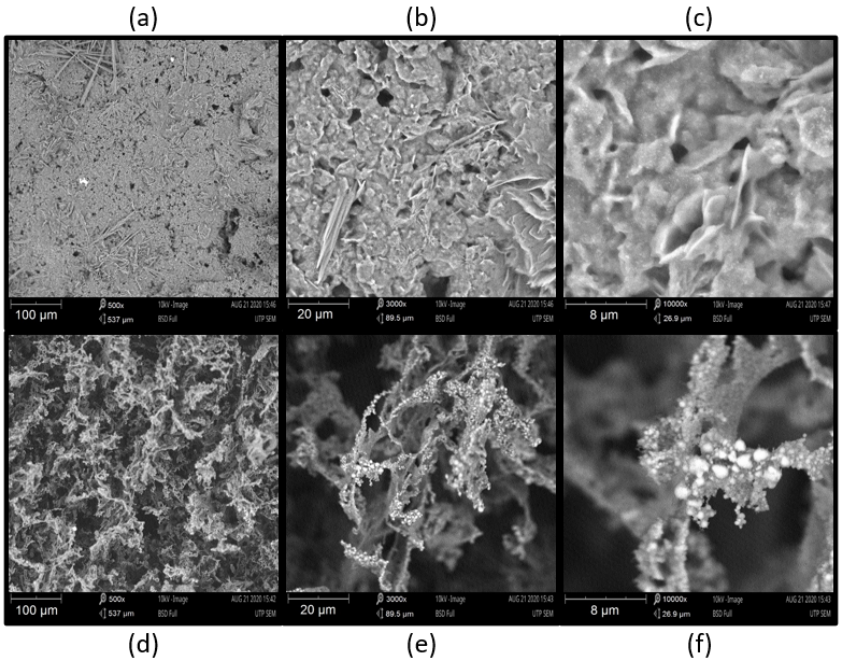

Fig. 3. SEM Imaging Microscopy of lignin-coated substrate versus OP-LSG. (a), Lignin at 100 µm resolution. (b), Lignin at 20 µm resolution. (c), Lignin at 8 µm resolution. (d), OP-LSG at 100 µm resolution. (e), OP-LSG at 20 µm resolution. (f) OP-LSG at 8 µm resolution.

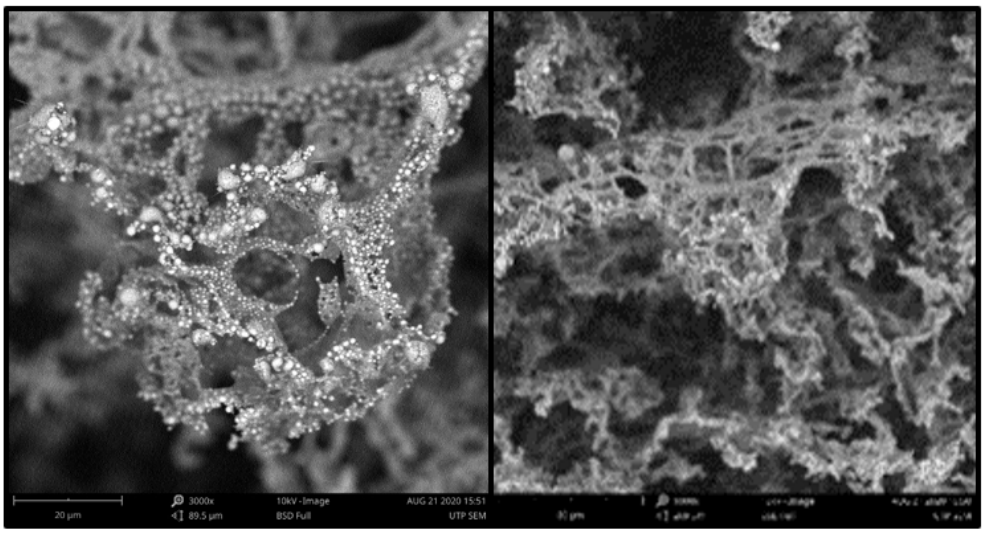

Fig. 4. SEM Imaging Microscopy of OP-LSG at (a), 20 µm resolution. (b), 80 µm resolution.

the lignin molecules, which converts the sp^3 carbon atoms in the lignin molecular structure into sp^2 carbon atoms. The heat generated by the localized laser beam initiates the carbonization process, which causes the oxygen functional group to burn off from the graphene oxide bonding, resulting in a reduced three-dimensional graphene oxide structure [13,23,43]. This can be seen in Fig. 4 (a) below, where the OP-LSG has a three-dimensional particle-like fibrous and porous structure, with some nanostructures. The presence of these pores in the OP-LSG makes it a good candidate for supercapacitor electrodes [40,44], as porous structures increase the specific surface area of the material, which is essential for ion diffusion and facilitates a higher surface contact area between the

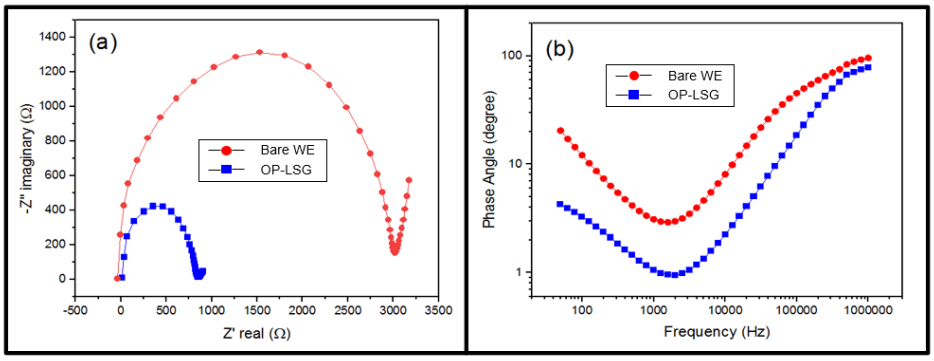

Fig. 5. Electrochemical Impedance Spectroscopy of OP-LSG versus bare carbon Working Electrode. (a), Nyquist plot (b), Phase angle versus frequency plot

electrolyte and the electrode [45–47].

As can be seen in Fig. 4 (b) above, OP-LSG has a unique surface topology and morphology, as compared to the rGO derived from kraft lignin [23] and pulpwood lignin [24], although a similar laser lithography process was employed. The FESEM images of both kraft lignin and pulpwood lignin-derived rGO indicate the presence of a sheet-like structure with large pores. In comparison, OP-LSG has a fibrous surface topology with nanoparticle fibers and dense, compact pores. This would indicate a higher specific surface area for the OP-LSG, as compared to the other two rGOs. This would translate to better performance as a supercapacitor electrode.

As for the electrochemical performance of the cell, Fig. 5 above shows the Nyquist plot and the phase angle *versus* the frequency plot of OP-LSG from the EIS, compared to the bare carbon WE. The Nyquist plot indicates the impedance of the material from 1 MHz to 10 Hz. Based on the plot, OP-LSG WE have a much lower resistance than the bare carbon WE. The three-dimensional porous and fibrous structure has contributed to much higher conductivity, as evidenced by the significant drop in impedance. This is possibly due to the higher rate of electron transfer, as compared to the carbon WE.

The OP-LSG has a lower phase shift as compared to the carbon WE based on the phase angle *versus* frequency plot. This would translate to lower power loss for the OP-LSG electrode, as compared to the bare electrode of the SPE. A supercapacitor with an OP-LSG electrode could potentially have lower power consumption, with a better power factor. Additionally, since the phase shift is lower, the response time of the OP-LSG electrode will also be faster than the bare carbon electrode, due to the lower lagging factor.

The Cyclic Voltammetry (CV) curves for the OP-LSG electrode under various scan rates from 0.01 V/s to 0.5 V/s, as shown in Fig. 6 above, provide insights into the electrochemical properties of the electrode in the electrolyte solution at different potentials. The CV curves exhibited a quasi-rectangular shape, as expected of an EDLC supercapacitor, at scan rates of 0.01 V/s to 0.1 V/s. At a scan rate of 0.2 V/s, the curve has a quasi-rectangular shape, but with a more prominent 'hump'. This is probably attributed to the saturation of ion concentration at the electrode surface as the potential increased. However, at a scan rate of 0.5 V/s, the curve appears to narrow, with a sharp-pointed tip near the 1.0 V potential. This likely indicates that the point of electrolysis has plateaued, and the supercapacitor has started behaving akin to a pseudocapacitor. This could mean the capacitance is due to the electrolyte, rather than the electrode as expected of an EDLC supercapacitor, with the electrode undergoing an oxidation and reduction process in the electrolyte [48].

Table 1 below shows the specific capacitances of OP-LSG at different CV scan rates. OP-LSG has the highest specific capacitance of 108 044 μF/cm^2 at a scan rate of 0.01 V/s. At a higher scan rate of 0.5 V/s, the specific capacitance decreases to 627 μF/cm^2. This is due to the reduction in the diffusion of ions into the electrode pores at higher scan rates, hence reducing the contact area between electrode and electrolyte [23,49]. However, the specific capacitance of OP-LSG is still higher than other lignin precursor supercapacitors such as Kraft lignin, which has a specific capacitance of 880.25 μF/cm^2 at a scan rate of 0.01 V/s [23].

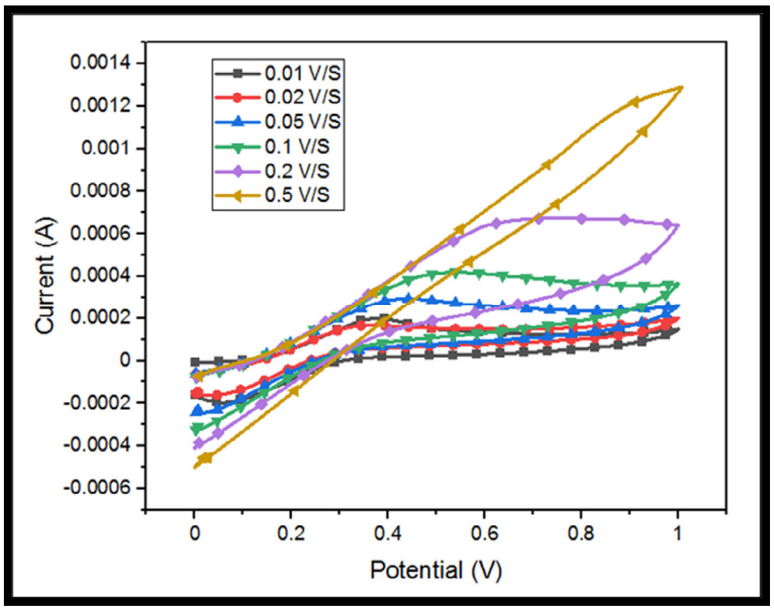

Fig. 6. Cyclic Voltammetry curve of the OP-LSG electrode collected at scan rates from 0.01 to 0.5 V/s.

Table 1. Specific capacitance of OP-LSG coated electrode at different CV scan rates, 0.1257 cm^2 electrode area, and a 1V voltage window.

Scan Rate	Area of CV Curve	Areal Specific Capacitance
0.01 V/s	2.72 x 10^{-4} AV	108044 μF/cm^2
0.02 V/s	2.09 x 10^{-4} AV	41619 μF/cm^2
0.05 V/s	2.04 x 10^{-4} AV	16235 μF/cm^2
0.1 V/s	1.48 x 10^{-4} AV	5886 μF/cm^2
0.2 V/s	1.17 x 10^{-4} AV	2335 μF/cm^2
0.5 V/s	7.88 x 10^{-4} AV	627 μF/cm^2

Fig. 7 above shows the Galvanostatic Charge-Discharge (GCD) curve of the OP-LSG electrode, to determine the charge-discharge characteristics of the electrode, besides the electrode's energy density, power density, and capacitance retention rate. Based on the GCD curve, at current densities of 0.01 and 0.05 A/cm^2, the curve is triangular, indicating the effective ion deposition on the OP-LSG electrode surface and interface of the ferrocyanide electrolyte. At current densities of 0.0001 to 0.005 A/cm^2, the curves have nonlinear profiles, due to internal resistance in the electrode [50]. This could most likely be caused by lignin molecules that were not fully carburized during the laser lithography process, due to the thick lignin coating on the glass substrate.

The supercapacitor's energy density and power density at different scan rates are listed in Table 2 above. The supercapacitor achieved a maximum energy and power density of 15 μWh/cm^2 and 597 μW/cm^2 at a scan rate of 0.01 V/s.

The GCD curves were further plotted to determine the characteristics of the supercapacitor for a charge-discharge cycle in order to determine its cycling stability. Fig. 8 Inset (a) below shows the charge-discharge trend of the electrode at the 1st cycle, whereas Fig. 8 Inset (b) shows the charge-discharge trend at the 1000th cycle. The supercapacitor has a leaner curve for the 1000th cycle compared to the 1st cycle, which has a somewhat larger curve, indicating that the supercapacitor's charge-discharge rate has become faster after multiple charge-discharge cycles. This could be attributed to a reduction in the resistance of the electrode, due to losses in the lignin layer resulting in the internal structure of the OP-LSG electrode supporting more immediate ion transfer [10]. The specific capacitance was calculated at 380 μF/cm^2 for the 1st charge-discharge cycle and 372 μF/cm^2 for the 1000th cycle, giving a capacitance retention

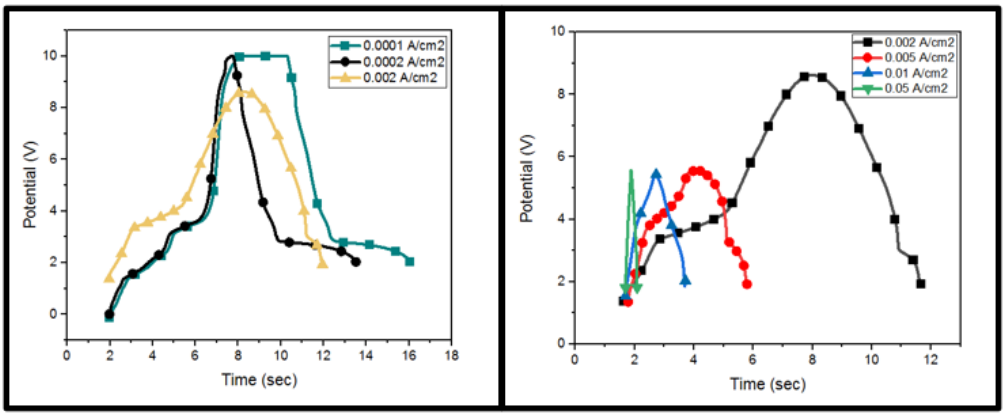

Fig. 7. Galvanostatic charge-discharge curve for the OP-LSG coated electrode

Table 2. Energy density and power density of OP-LSG coated electrode at different scan rates.

Scan Rate	Energy Density	Power Density
0.01 V/s	15.01 μWh/cm^2	596.93 μW/cm^2
0.02 V/s	5.78 μWh/cm^2	414.94 μW/cm^2
0.05 V/s	2.25 μWh/cm^2	423.89 μW/cm^2
0.1 V/s	0.82 μWh/cm^2	294.32 μW/cm^2
0.2 V/s	0.32 μWh/cm^2	166.76 μW/cm^2
0.5 V/s	0.09 μWh/cm^2	62.67 μW/cm^2

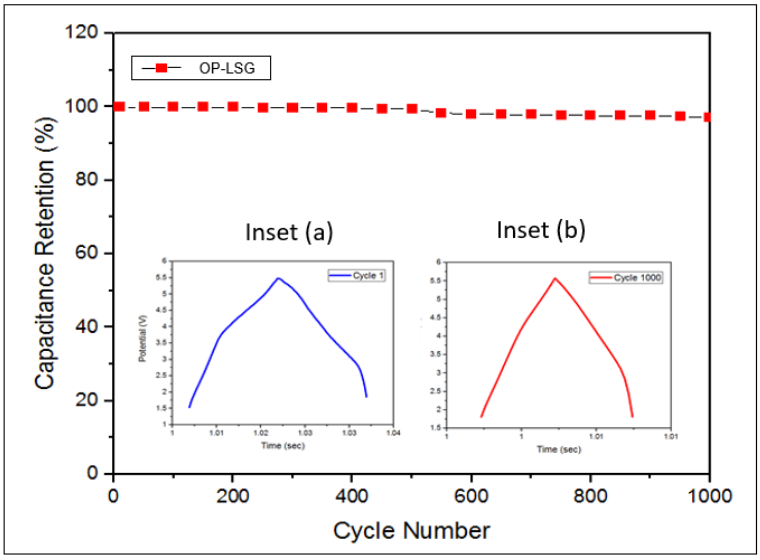

Fig. 8. Capacitance retention of OP-LSG for 1000 charge-discharge cycles. Inset (a), GCD Curve at 1st cycle. Inset (b), GCD curve at 1000th cycle.

rate of 97.8% over 1000 charge and discharge cycles. This can also be seen in Fig. 8 below, where the capacitance retention was constant for the first 500 cycles and started to drop slightly after the 500-cycle mark.

CONCLUSIONS

Laser lithography of oil palm lignin has successfully synthesized reduced Graphene Oxide (OP-LSG) with better physical and electrochemical properties compared to other lignin-derived

rGOs. This is because of OP-LSG's unique surface morphology consisting of a three-dimensional fibrous surface topology with nanoparticle fibers and dense, compact pores, unlike the sheet-like structures with large pores of the other lignin-derived rGOs. The fibrous nanoparticles with compact holes in the surface contribute to an overall higher surface area in OP-LSG. Based on the electrochemical performance analysis of the OP-LSG electrode in a three-electrode setup, OP-LSG has the highest specific capacitance of 108.044 mF/cm^2 at a scan rate of 0.01 V/s, with energy and power densities of 15 $\mu Wh/cm^2$ and 597 $\mu W/cm^2$ at a scan rate of 0.01 V/s. Moreover, the OP-LSG electrode retained 97.5% of its initial capacitance after 1000 charge-discharge cycles. OP-LSG is indeed an excellent material as a supercapacitor electrode due to its high performance in terms of specific capacitance, energy density, capacitance retention, and power density. Further optimization is required to achieve a power density comparable to graphene derived from commercial polymers such as polyimide.

CONFLICTS OF INTEREST

There are no conflicts to declare.

REFERENCES

1. Häggström F, Delsing J. IoT Energy Storage - A Forecast. Energy Harvesting and Systems. 2018;5(3-4):43-51.
2. Qi Z, Koenig GM. Review Article: Flow battery systems with solid electroactive materials. Journal of Vacuum Science & Technology B, Nanotechnology and Microelectronics: Materials, Processing, Measurement, and Phenomena. 2017;35(4):040801.
3. Ke Q, Wang J. Graphene-based materials for supercapacitor electrodes – A review. Journal of Materiomics. 2016;2(1):37-54.
4. Radamson, H.H., 2017. Graphene, In Springer Handb. Electron. Photonic Mater., S. Kasap, P. Capper, eds., Springer International Publishing, pp: 1173–1183.
5. Bhuyan MSA, Uddin MN, Islam MM, Bipasha FA, Hossain SS. Synthesis of graphene. International Nano Letters. 2016;6(2):65-83.
6. Geim AK. Graphene prehistory. Physica Scripta. 2012;T146:014003.
7. Balandin AA, Ghosh S, Bao W, Calizo I, Teweldebrhan D, Miao F, et al. Superior Thermal Conductivity of Single-Layer Graphene. Nano Letters. 2008;8(3):902-7.
8. Wei D, Liu Y, Wang Y, Zhang H, Huang L, Yu G. Synthesis of N-Doped Graphene by Chemical Vapor Deposition and Its Electrical Properties. Nano Letters. 2009;9(5):1752-8.
9. Ramachandran R, Felix S, Joshi GM, Raghupathy BPC, Jeong SK, Grace AN. Synthesis of graphene platelets by chemical and electrochemical route. Materials Research Bulletin. 2013;48(10):3834-42.
10. Bhattacharjya D, Kim C-H, Kim J-H, You I-K, In JB, Lee S-M. Fast and controllable reduction of graphene oxide by low-cost CO2 laser for supercapacitor application. Applied Surface Science. 2018;462:353-61.
11. Lee S-H, Kim JH, Yoon J-R. Laser Scribed Graphene Cathode for Next Generation of High Performance Hybrid Supercapacitors. Sci Rep. 2018;8(1):8179-.
12. Wen F, Hao C, Xiang J, Wang L, Hou H, Su Z, et al. Enhanced laser scribed flexible graphene-based micro-supercapacitor performance with reduction of carbon nanotubes diameter. Carbon. 2014;75:236-43.
13. Duy LX, Peng Z, Li Y, Zhang J, Ji Y, Tour JM. Laser-induced graphene fibers. Carbon. 2018;126:472-9.
14. Lin J, Peng Z, Liu Y, Ruiz-Zepeda F, Ye R, Samuel ELG, et al. Laser-induced porous graphene films from commercial polymers. Nature communications. 2014;5:5714-.
15. Wang Y, Zhu C, Pfattner R, Yan H, Jin L, Chen S, et al. A highly stretchable, transparent, and conductive polymer. Sci Adv. 2017;3(3):e1602076-e.
16. Jeszka JK, Ulański J, Kryszewski M. Conductive polymer: reticulate doping with charge-transfer complex. Nature. 1981;289(5796):390-1.
17. Zhao Y, Liu B, Pan L, Yu G. 3D nanostructured conductive polymer hydrogels for high-performance electrochemical devices. Energy & Environmental Science. 2013;6(10):2856.
18. Mastragostino M. Conducting polymers as electrode materials in supercapacitors. Solid State Ionics. 2002;148(3-4):493-8.
19. In JB, Hsia B, Yoo J-H, Hyun S, Carraro C, Maboudian R, et al. Facile fabrication of flexible all solid-state micro-supercapacitor by direct laser writing of porous carbon in polyimide. Carbon. 2015;83:144-51.
20. Zhang Y, Fan W, Huang Y, Zhang C, Liu T. Graphene/carbon aerogels derived from graphene crosslinked polyimide as electrode materials for supercapacitors. RSC Advances. 2015;5(2):1301-8.
21. Pisareva TA, Kharanzhevskii EV, Reshetnikov SM. Synthesis of nanocrystalline graphite for supercapacitor electrodes by short-pulse laser processing of a polyimide film. Russian Journal of Applied Chemistry. 2016;89(6):897-903.
22. Prado GHC, Prado IM. Hydrogels Based on Natural Polysaccharides and Their Applications. Comprehensive Glycoscience: Elsevier; 2021. p. 71-92.
23. Mahmood F, Zhang H, Lin J, Wan C. Laser-Induced Graphene Derived from Kraft Lignin for Flexible Supercapacitors. ACS Omega. 2020;5(24):14611-8.
24. Lei Y, Alshareef AH, Zhao W, Inal S. Laser-Scribed Graphene Electrodes Derived from Lignin for Biochemical Sensing. ACS Applied Nano Materials. 2019;3(2):1166-74.
25. Xiong C, Zhong W, Zou Y, Luo J, Yang W. Electroactive biopolymer/graphene hydrogels prepared for high-performance supercapacitor electrodes. Electrochimica Acta. 2016;211:941-9.
26. Cao KLA, Kitamoto Y, Iskandar F, Ogi T. Sustainable porous hollow carbon spheres with high specific surface area derived from Kraft lignin. Advanced Powder Technology. 2021;32(6):2064-73.
27. Tai MJY, Perumal V, Gopinath SCB, Raja PB, Ibrahim MNM, Jantan IN, et al. Laser-scribed graphene nanofiber decorated with oil palm lignin capped silver nanoparticles: a green biosensor. Sci Rep. 2021;11(1):5475-.
28. Childres, I., L.A. Jauregui, W. Park, H. Caoa and Y.P. Chena, 2013. Raman spectroscopy of graphene and related materials, In New Dev. Phot. Mater. Res., , pp: 403–418.

29. Lee PT, Lowinsohn D, Compton RG. The use of screen-printed electrodes in a proof of concept electrochemical estimation of homocysteine and glutathione in the presence of cysteine using catechol. Sensors (Basel). 2014;14(6):10395-411.
30. Ndiaye AL, Delile S, Brunet J, Varenne C, Pauly A. Electrochemical Sensors Based on Screen-Printed Electrodes: The Use of Phthalocyanine Derivatives for Application in VFA Detection. Biosensors (Basel). 2016;6(3):46.
31. Elgrishi N, Rountree KJ, McCarthy BD, Rountree ES, Eisenhart TT, Dempsey JL. A Practical Beginner's Guide to Cyclic Voltammetry. Journal of Chemical Education. 2017;95(2):197-206.
32.Wu, J., X.Z. Yuan and H. Wang, 2011. Cyclic voltammetry. PEM Fuel Cell Diagnostic Tools, (d): 71–85.
33. Strong V, Dubin S, El-Kady MF, Lech A, Wang Y, Weiller BH, et al. Patterning and Electronic Tuning of Laser Scribed Graphene for Flexible All-Carbon Devices. ACS Nano. 2012;6(2):1395-403.
34. Rao S, Kanaka Durga I, Naresh B, Jin-Soo B, Krishna TNV, In-Ho C, et al. One-Pot Hydrothermal Synthesis of Novel Cu-MnS with PVP Cabbage-Like Nanostructures for High-Performance Supercapacitors. Energies. 2018;11(6):1590.
35. Tai MJY, Vasudevan M, Perumal V, Liu WW, Mohamed NM. Synthesis of Laser Scribed Graphene Electrode with Optimized Power for Biosensing. 2019 IEEE Regional Symposium on Micro and Nanoelectronics (RSM); 2019/08: IEEE; 2019.
36. Malard LM, Pimenta MA, Dresselhaus G, Dresselhaus MS. Raman spectroscopy in graphene. Physics Reports. 2009;473(5-6):51-87.
37. Lamberti A, Perrucci F, Caprioli M, Serrapede M, Fontana M, Bianco S, et al. New insights on laser-induced graphene electrodes for flexible supercapacitors: tunable morphology and physical properties. Nanotechnology. 2017;28(17):174002.
38. Casiraghi C, Hartschuh A, Qian H, Piscanec S, Georgi C, Fasoli A, et al. Raman Spectroscopy of Graphene Edges. Nano Letters. 2009;9(4):1433-41.
39. Gawlik G, Ciepielewski P, Baranowski J. Study of Implantation Defects in CVD Graphene by Optical and Electrical Methods. Applied Sciences. 2019;9(3):544.
40. Gong Y, Li D, Luo C, Fu Q, Pan C. Highly porous graphitic biomass carbon as advanced electrode materials for supercapacitors. Green Chemistry. 2017;19(17):4132-40.
41. Cusola O, Kivistö S, Vierros S, Batys P, Ago M, Tardy BL, et al. Particulate Coatings via Evaporation-Induced Self-Assembly of Polydisperse Colloidal Lignin on Solid Interfaces. Langmuir. 2018;34(20):5759-71.
42. Javed A, Ullsten H, Rättö P, Järnström L. Lignin-containing coatings for packaging materials. Nordic Pulp & Paper Research Journal. 2018;33(3):548-56.
43. El-Kady MF, Strong V, Dubin S, Kaner RB. Laser Scribing of High-Performance and Flexible Graphene-Based Electrochemical Capacitors. Science. 2012;335(6074):1326-30.
44. Chai H, Peng X, Liu T, Su X, Jia D, Zhou W. High-performance supercapacitors based on conductive graphene combined with Ni(OH)2 nanoflakes. RSC Advances. 2017;7(58):36617-22.
45. Khan A, Senthil RA, Pan J, Osman S, Sun Y, Shu X. A new biomass derived rod-like porous carbon from tea-waste as inexpensive and sustainable energy material for advanced supercapacitor application. Electrochimica Acta. 2020;335:135588.
46. Beduk T, Ait Lahcen A, Tashkandi N, Salama KN. One-step electrosynthesized molecularly imprinted polymer on laser scribed graphene bisphenol a sensor. Sensors and Actuators B: Chemical. 2020;314:128026.
47. Li H, Zhao Y, Liu S, Li P, Yuan D, He C. Hierarchical porous carbon monolith derived from lignin for high areal capacitance supercapacitors. Microporous and Mesoporous Materials. 2020;297:109960.
48. Qi D, Liu Z, Liu Y, Leow WR, Zhu B, Yang H, et al. Suspended Wavy Graphene Microribbons for Highly Stretchable Microsupercapacitors. Advanced Materials. 2015;27(37):5559-66.
49. Xu Y, Lin Z, Zhong X, Huang X, Weiss NO, Huang Y, et al. Holey graphene frameworks for highly efficient capacitive energy storage. Nature Communications. 2014;5(1).
50. Romanitan C, Varasteanu P, Mihalache I, Culita D, Somacescu S, Pascu R, et al. High-performance solid state supercapacitors assembling graphene interconnected networks in porous silicon electrode by electrochemical methods using 2,6-dihydroxynaphthalen. Sci Rep. 2018;8(1):9654-.